LA-UR- 93-2213

Title:	Design and Implementation of Low-Q Diffractometers at Spallation Sources
Author(s):	P.A. Seeger, R.P. Hjelm
Submitted to:	ACA Symposia Proceedings

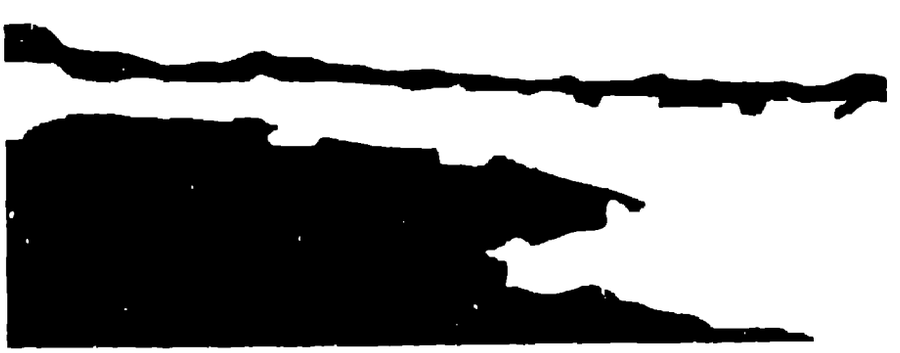

Los Alamos
NATIONAL LABORATORY

LA-UR-93-2213

Design and Implementation of Low-Q Diffractometers at Spallation Sources

Philip A. Seeger and Rex P. Hjelm

Los Alamos Neutron Scattering Center
Los Alamos National Laboratory, Los Alamos, NM 87545-1663

American Crystallographic Association Symposia Proceedings
Albuquerque, NM, 24-28 May, 1993

DESIGN AND IMPLEMENTATION OF LOW-Q DIFFRACTOMETERS AT SPALLATION SOURCES

Philip A. SEEGER and Rex P. HJELM

Los Alamos Neutron Scattering Center
Los Alamos National Laboratory
Los Alamos, NM 87545–1663, USA.

Low-Q diffractometers at spallation sources that use of time of flight methods have been successfully implemented at several facilities, including the Los Alamos Neutron Scattering Center. The proposal to build new, more powerful, advanced spallation sources using advanced moderator concepts will provide luminosity greater than 20 times the brightest spallation source available today. These developments provide opportunity and challenge to expand the capabilities of present instruments with new designs. We review the use of time of flight for low-Q measurements and introduce new designs to extend the capabilities of present-day instruments. We introduce Monte Carlo methods to optimize design and simulate the performance of these instruments. The expected performance of the new instruments are compared to present day pulsed source- and reactor-based small-angle neutron scattering instruments. We review some of the new developments that will be needed to use the power of brighter sources effectively.

1. INTRODUCTION

The development of pulsed spallation sources as alternative sources to reactors for neutron scattering measurements has increased the availability of neutron scattering instruments for condensed matter research and nuclear physics world-wide. The facilities at Rutherford (ISIS) in the UK, Los Alamos (LANSCE) and Argonne (IPNS)

National Laboratories in the USA and at KENS in Japan have led to new instrumentation based on the use of time-of-flight (TOF) techniques in various scattering measurements. It is likely that future neutron sources will be this type, as they are less costly than reactors, and safety and environmental concerns are less severe than for reactors, Thus it is highly important to consider carefully what can be done with spallation neutron sources.

The concern here is the implementation of TOF methods for small-angle neutron scattering (SANS) instruments at pulsed spallation sources and the development of new instrumentation for more intense pulsed spallation sources (IPSS) in the future. The large demand for small-angle instruments to probe structure in condensed matter at intermediate and long length scales dictates that several such instruments be built at any new facility.

TOF techniques remove the need for monochromation of the incident beam; thus a broad band of neutron wave lengths can be employed, using the TOF to measure the incident wavelength, λ, of each detected neutron, This is important, as spallation sources do not have the total neutron luminosity of the more powerful reactors. The very short duration of the neutron pulse not only makes TOF measurement easy, but the proper use of TOF methods makes instruments at pulsed spallation sources competitive with their steady-state counterparts. In fact, we have demonstrated that a SANS instrument at the brightest spallation source, LQD at LANSCE, is comparable in many respects with D11 [1,2].

Basic and technical issues have to be addressed in implementing low-angle instruments on pulsed sources. Some of these issues are common with instruments at reactors, but others are unique. Many of these have been addressed successfully, and their solutions have been described in a number of publications [1–10]. Others are still not solved; further, the development of instruments at new brighter sources presents some new challenges.

Here we discuss some of the issues and their solutions. Our discussion includes design criteria for TOF-SANS instruments, the effect of gravity on the longer wavelength neutrons, and possible effects due inelastic (or quasielastic) scattering. We go on to consider the requirement that the raw data, acquired as large three-dimensional his

tograms in x, y and TOF, be remapped into meaningful momentum transfer coordinates. The mapping onto is many-to-one, and the quality of the information varies over the raw histogram. This implies a need to devise schemes to use the data most effectively and a need to provide the user with a convenient and effective means of manipulating the reducing the data. We introduce the highly important R & D issue of detector development needed for the high instantaneous data rates at an IPSS. Finally, we discuss the performance expected of new designs for TOF-SANS instruments for an IPSS with a discussion on how these instruments are likely to perform in comparison with D11 at the Institut Laue-Langevin (ILL).

2. SOURCES

The short duration of neutron pulses available at spallation sources makes the TOF measurement easy, and allows the use of every available moderated neutron for a measurement. This allows the performance of spallation-based instruments to compare favorably with steady state instruments even though the luminosity, $\Lambda(\lambda)$ (neutrons/Å/sterad/cm^2/s), is considerably lower with present pulsed spallation sources and moderators. The total flux at the sample, Φ (neutrons/cm^2/s), integrated over λ, may be used (subject to requirements of the measurement, discussed below). In the small-angle scattering experiment, we are interested in small momentum transfers, Q. The relationship between scattering angle, 2θ, and incident neutron wavelength is

$$Q = \left(\frac{4\pi}{\lambda}\right) \sin\theta \approx \frac{4\pi\theta}{\lambda} \qquad (1)$$

where the approximation holds only for small θ. We see that low Q is obtained for long wavelengths as well as small angles. Thus low-Q is best attained using a moderator with higher $\Lambda(\lambda)$ at long wavelengths - a cold moderator must be coupled to the neutron production target.

LQD at LANSCE uses a liquid hydrogen moderator in flux-trap geometry relative to a split tungsten target [11]. Moderators for the IPSS will also be liquid hydrogen, but will be of a new design that will lead to increased Φ by coupling the cold

moderator with a reflector and possibly including an ambient temperature water premoderator [12–14]. The pulse widths will be increased up to 300–500 μs with the new designs, but will not significantly affect the resolution of low-Q instruments. The gains afforded by these strategies could be significant, as coupling alone is likely to afford an increase in at thermal energies by a factor of four. Combined with the likely 5-fold increase in neutron production from the target, roughly a 20-fold increases in neutron production compared to the present LANSCE should result.

3. INSTRUMENTS

Present spallation SANS instrumentation has concentrated on the middle Q-ranges. For example, our present LANSCE LQD accesses Q from 0.002 to 0.4 $Å^{-1}$. With the promise of higher neutron fluxes, a new challenge exits to extend the range of Q both to lower and higher values, in order to probe larger and smaller length scales than presently possible. A very-low-Q instrument, VLQD, measuring Q between 0.0007 and 0.1 $Å^{-1}$, would provide overlap with light scattering measurements and x-ray and neutron cameras having Bonse-Hart geometry, and would be would be useful in metallurgy, materials science, self assembling systems and polymers, just as a few examples. At the other end of the scale are structural problems in colloids and polymers, fluids, and composite materials that require large Q-values, overlapping with the domain of diffractometers for liquids and amorphous materials and crystalline powders. This Q-domain would be accessed by an MQD designed to take measurements from 0.005 to 2.0 $Å^{-1}$. The middle Q-range of present instrumentation will still be the most important, and the planned next generation of mid-Q-range instruments, here designated LQD and Biology LQD, will access Q from 0.001 to 0.3 $Å^{-1}$.

The brightness of the sources will enable faster data acquisition, making time-dependent studies possible (a new area for SANS), and enabling work on small volumes and special environments. In addition, measurements will be extended to systems with scattering intensities too weak to be considered practical with present instruments. The increased intensity also presents opportunity to develop hybrid instruments that measure scattering currently measured by several different instrument types, for example,

the WINK instrument at KEK simultaneously measures small-angle scattering and powder diffraction [15]. Hybrid instruments allow characterization of physical states on very different length scales, making clearer the inter-relationships among these states. Although details of these enhancements are not included in our present discussion, they will be considered in any final proposal.

[figure 1 here]

3.1 Geometry of Low-Q Instruments

Figure 1 illustrates the general instrument geometry which has been used in the design and analysis of this family of SANS instruments . The most significant variables are the total instrument length D_T, the sample-to-detector distance L_2, and the maximum wavelength λ_{max}. (Moderator-to-sample distance is $L_1 = D_T - L_2$.) The search for an optimum is carried out using Monte Carlo methods (discussed in section 5 below) over these three variables, by choosing the minimal value of Q to be measured and optimizing at a single Q-value at about 3 times Q_{min}. Other elements that can be adjusted are the entrance aperture of the collimator (radius R_1, located distance D_1 from the moderator), the massive T_0 chopper (distance D_t from the moderator), the disk frame-definition chopper (distance D_f from the moderator), the collimator exit aperture (radius R_2, distance D_2 from moderator, and attached to the gravity focuser if one is used), and the beamstop size (radius R_b). The T_0 chopper is required in these applications to keep the initial flash of hot neutrons and γ-radiation from entering the instrument and to act as a low-energy-pass filter for the incident beam. The gravity focuser which moves upward by a distance Y_0 during each beam pulse is used to select trajectories (as a function of λ^2) that will all strike the detector at its center. The stroke is a function of flight path ratios and λ_{max}, and tends to be about a third of the beam droop that would otherwise occur at λ_{max}. The derived dimensions of three instruments designed for a 330 kW (proton beam) source operating at 20 Hz are given in Table 1 and the computed minimum Q-values in Table 2. The LANSCE LQD, which operates on the present LANSCE target at 60 to 80 kW and 20 Hz, is included for comparison

TABLE 1

Dimensions for Low-Q Instruments at an Intense Pulsed Spallation Source

Instrument	D_1 (m)	R_1 (mm)	D_t (m)	D_f (m)	D_2 (m)	R_2 (mm)	L_1 (m)	D_T (m)	R_b (mm)
LANSCE	4.535	7.66	—	—	8.222	4.21	8.360	12.72	20.7
MQD	4.500	7.91	—	—	6.880	5.40	7.000	12.00	36.0
LQD	4.600	7.98	5.0	9.00	9.85	5.61	10.00	19.00	39.9
VLQD	4.600	19.82	5.0	23.00	23.85	11.03	24.00	48.00	—

TABLE 2

Parameters for Low-Q Instruments at an Intense Pulsed Spallation Source

Instrument	θ_{min} (mrad)	λ_{max} (Å)	Q_{min} (Å^{-1})	Y_G (mm)
LANSCE LQD	4.8	15.2	0.002	1.2
MQD	7.2	16.0	0.003	1.0
LQD	4.4	20.0	0.0015	6.0
VLQD	2.2	20.5	0.0007	—

3.2 Collimation, Optimization, and Resolution

The direction of the beam momentum is defined by collimation using two pinholes. The collimator geometry is determined by optimization of the intensity and resolution (precision in θ). These are related by the usual relationships for pinhole geometry, and assuming isotropic scatter (scalar momentum transfer),

$$\delta I_n = K\Lambda(\lambda)\Delta\lambda_n\left(\frac{\pi R_1 R_2}{L_1}\right)^2\frac{\Delta x_d \Delta y_d}{L_2^2} \qquad (2)$$

for intensity, δI_n, in the n^{th} time channel, and

$$V_d[\theta] = \frac{1}{12}\left[\frac{3R_1^2\left(D_T - D_2\right)^2 + 3R_2^2\left(D_T - D_1\right)^2}{L_c^2 L_2^2} + \frac{\Delta x_d^2 + \Delta y_d^2}{2L_2^2}\right] + V[c] \qquad (3)$$

for the variance in the scattering angle, 2θ in the d^{th} spatial (detector) channel [16–18]. Dimensions in addition to those defined in figure 1 are $L_c = D_2 - D_1$, the collimator length, and Δx_d and Δy_d, which refer to the x and y dimensions of the d^{th} detector element. In our case the locations of events on the area detector (see below) are encoded by calculation of the signal centroid, which contributes variance V[c] to the resolution.

The optimization procedure is to minimize the variance, V_d, while holding the intensity, δI, constant, or equivalently to maximize δI while holding V_d constant. Very generally, the aperture terms in equation (3) should be made equal, accomplished by making the radii proportional to t distance from the detector (the "cone" rule). We are limited, however, by attainable detector resolution; the next to last term in equation (3) can thus only be made smaller by increasing L_2 and subsequently the total length. In fact the best optimization of count rate and resolution is obtained by lengthening the instrument as much as possible and scaling R_1 and R_2 with the total length. However, the total length is also limited, either by the size of the experimental hall, the total solid angle of the moderator as seen from the detector, the available sample area, or (for a pulsed source) by the "frame overlap" condition of fast neutrons from a subsequent pulse catching up with the slow, long-wavelength neutrons. In low-Q the latter are important as seen in equation (1), and since low Q-values require long total flight paths, the frame overlap condition is avoided by the addition of a frame-definition chopper (figure 1), which also defines the bandwidth used in the instrument. Minimizing penumbras leads to placing the moderator relatively close to the collimator, and likewise minimizing the gap between the collimator and the sample. Intensity at the detector can be increased without sacrificing resolution by increasing the number of collima-

tor apertures. Provision is made for multiple pinholes (figure 1) with intermediate baffles to prevent crosstalk [9] in all instruments but VLQD.

3.3 The Effect of Gravity

Over the total length of the instrument the neutron falls under the force of gravity: the slower neutrons fall the greater distance. This results in substantial loss in resolution in the vertical direction of the machine [19]. The solution with shorter instruments is to use a collimator exit aperture (figure 1) that is moved upward at constant acceleration during the course of a TOF frame to select those neutrons with sufficiently high arch (proportional to λ^2) to hit the center of the detector (at the beam stop). Such a device has been implemented on the present LQD [9], and is planned for the new LQD and MQD.

In a long instrument such as VLQD, the slow neutron trajectories have such a high arch through the collimator that the intermediate baffles indicated in figure 1 are not practical (limiting the instrument to a single aperture). Also, the vertical motion required for the gravity focuser would be too large (56 mm!), so the VLQD is assumed not to have gravity focus. All of the transmitted neutrons in the wavelength band of interest will droop *below* the beamstop, which will thus only intercept neutrons which scatter upward. We therefore plan to omit the beamstop in the VLQD. However, since the wavelength bandpass is small, an adjustable beamstop could be included.

In assessing the resolution of D11 at its maximum length of 76 m, we discovered that the effect of gravity is deleterious at a continuous source instrument. The velocity of a 12-Å neutron is 329.7 m/s, so the flight time is 0.234 s and the neutron falls 269 mm due to gravity. Parabolic trajectories defined as being on-axis at the entrance and exit of the collimation strike the detector below axis by an amount proportional to λ^2—specifically 0.84 mm/Å^2. The resulting average droop of 121 mm is not in itself significant, but the variance of vertical position on the detector resulting from the spread of wavelengths of the $\Delta\lambda/\lambda$ = 10% velocity selector is the dominant term in the Q-resolution for any value of $Q \leq 0.002$ Å^{-1}. Thus the possibility to extend the Q-range below about 0.002 Å^{-1} is very limited at a steady-state source. A narrower velocity spectrum could be used, at the expense lowering the already meager count rate .

At a pulsed source, on the other hand, correcting for gravitational droop is trivial, because the time-of-flight of each neutron *is* measured and the droop is easily calculated. Therefore gravity does not limit the instrument length nor the wavelength range which may be used.

3.4 Detectors

One of the most important issues for time-of-flight instrumentation is the development of new fast detectors and encoding schemes. Present gas detectors can be made to handle the peak instantaneous count rates at present sources, but new designs will be needed to deal with peak intensities envisioned at the brightest sources under consideration. Thus detector development is one of the most critical R & D issues that must presently be addressed.

Because of the wide dynamic range afforded by the TOF technique, detectors can be fixed in position. Thus the collimation can be optimized with respect to both intensity and Q-precision. Further, fixed baffles can be installed in scattering flight path tube to reduce backgrounds.

4. DATA REDUCTION

4.1 Intensity Map

Implementation of TOF techniques on a small-angle instrument requires mapping of the three-dimensional histograms of detector x, y and TOF into intensity as a function of either scalar or vector momentum transfers. Figure 2 gives an example of raw data from a vycor glass sample, PT5, *vs.* TOF and radial position on the detector. To allow visualization, the 2-dimensional detector is reduced to one dimension by averaging over annular zones of width equal to one pixel. The characteristic spinodal scattering peak ($Q = 0.02$ Å^{-1}) is distorted in intensity by the incident beam spectrum, and moves outward on the detector at later times. The master equation for mapping, in absolute differential scattering probability, is

$$\frac{dP(Q_k)}{d\Omega} = \frac{\sum_{\{n,d\}=k} N_{n,d}}{\sum_{\{n,d\}=k} \Phi_n \Omega_d} \qquad (4)$$

where the sums are over the set of time (n) and spatial (d) channels that contribute to the k^{th} Q-bin according to the relation $Q_k = (4\pi/\lambda_n) \sin \theta_d$. Equation (4) take into account that the counts in any n,d cell, $N_{n,d}$, must be weighted by the number of counts that would have been measured in that cell, $\Phi_n\Omega_d$, in order to optimize the information content in Q from the counts in each cell [1,5–7]. Normalization is then given by a similar sum of products of measured transmitted beam in each time channel, Φ_n, with the solid angle subtended by the spatial channel, Ω_d. All relevant corrections, such as detector nonlinearity [1], are made to $N_{n,d}$ before summing. Equation (4) implies very careful measurement of Φ properly normalized for $\Lambda(\lambda)$ by comparison with some scatterer of known $dP/d\Omega$ [20,21]. Conversion of $dP/d\Omega$ to the more usual macroscopic differential cross section per unit scattering volume, $d\Sigma(Q)/d\Omega$ (cm^{-1}), is made by dividing equation (4) by the sample path length. The propagation of errors defining the uncertainties in $dP/d\Omega$ is straightforward using the usual methods, but *must* be done at every step in parallel with the corrections and normalizations.

[figure 2 here]

4.2 Q-precision of the map

Each n,d cell also caries with it different information on Q. The contribution of each cell to the variance in Q is

$$V_{n,d}[Q] = \bar{Q}^2_{n,d}\left[\frac{V_d[\theta]}{\bar{\theta}^2_d} + \frac{V_n[t]}{\bar{t}^2_n}\right] \qquad (5)$$

where bars are used to express explicitly that values are averaged over cells. The variance of the TOF values, t, in the n^{th} channel is $V_n[t]$, and $V_d[\theta]$ is given by equation (3). Equation (5) shows why a "logarithmic" TOF binning scheme is preferred in data acquisition, as $V_n[t]/\bar{t}_n^2 = \frac{1}{12}(\Delta t/t)^2$ = constant, which can be set to match the smallest value of the d-channel term in equation (5).

The precision in Q in each bin as a consequence of combining cells is calculated using the relation

$$V_k[Q] = \overline{V_{\{n,d\}=k}[Q]} + V\left[\overline{Q_{\{n,d\}=k}}\right] \qquad (6)$$

which means that the variance of the k^{th} Q-bin is the sum of the average variances of the n,d cells (given in each case by equation (5)) in the bin and the variance of the various Q's included in the bin. The cells are combined according to the weighting discussed in introducing equation (4); thus the information content in $dP/d\Omega$ is coupled with that in Q.

Equation (6) suggests an additional weighting factor which may be included in the mapping, as one may wish to exclude cells whose contribution to the total variance is excessive when compared to the variance from the Q-bin width. Thus a selection criterion is used to determine whether a cell should be used in the mapping. This is given by

$$V_{n,d}[Q] \le \frac{f}{12}\Delta Q_k^2 \qquad (7)$$

where f relates the maximum acceptable cell variance to the Q-bin variance. Usually we choose f = 1.5, but we can trade intensity for resolution by using a larger value. Equations (4) through (6) imply further that the size of the Q bins, ΔQ, should be a function of Q. We have verified by calculation an appropriate binning algorithm for the present LQD: For $Q < 0.006$ Å^{-1} the bin widths should increase with Q as $\Delta Q/Q = 0.167$. The bins should then have constant width of $\Delta Q = 0.001$ Å^{-1} in the domain

$0.006 \leq Q \leq 0.04$ Å^{-1}. They should increase again with Q above this value with $\Delta Q/Q = 0.025$. This "log-lin-log" scheme is practical only for maps (one- or two-dimensional) that have the radial component of Q as an independent variable.

[figure 3 here]

In figure 3 are the results of the transformation of the PT5 data as a map of Q and λ. In this transformation a similarly transformed background was subtracted from the sample scattering. The invariance in Q is illustrated by the horizontal distribution in intensity, as it should be. The variation in V[Q] with λ is seen as the widening of the band at shorter wavelengths. All the values below the line are removed, according to the criterion expressed in equation (7). The final map is shown as a radial average in figure 4. The success of the instrument and of the data analysis is shown by our recent results comparing a measurement of this sample on LQD and on D11 at 10 and 20 m source to detector distance [1,2]. The measured $dP/d\Omega$ were the same on the two instruments, as was the quality of the data. The measurement on LQD on a 60 kW source took three times as long as that on D11, but the data on LQD extends from 0.003 to 0.25 Å^{-1}, whereas that from D11 extended from 0.005 to 0.05 Å^{-1}. Thus LQD afforded a significantly larger dynamic range.

[figure 4 here]

4.3 Quasi-elastic/Inelastic Effects

We have mentioned in passing corrections made to the data. We have outlined some of these in a recent publications [1]. One that deserves further effort is moderation of the scattered neutron by the sample [7]. The consequences of this are not yet fully understood, but for samples in water, the likely result is considerable sample-dependent background. Some recent measurements [22,23] and a proposed modeling method [24] have been published. Further effort is needed to understand the importance of these dynamic effects to TOF–SANS.

5. MONTE CARLO SIMULATIONS OF INSTRUMENT PERFORMANCE

In order to understand the capabilities of the new instrumentation, we have done an extensive study on their performance using Monte Carlo simulation techniques. To test the validity of the Monte Carlo procedure, we have also simulated the PT5 measurement (figures 2–4), using it as a benchmark to evaluate critically the correctness of the simulation. We then use this properly normalized simulation to extrapolate to the performance of the new instruments that we will build at an IPSS. There are two aspects of the performance of these instruments that we want to address —the precision in Q of the measurement and the flux at the sample scaled in a manner that reflects the expected count rate as detected by the instrument.

The Monte Carlo simulations of pulsed spallation source instrument performance include wavelength-dependent effects from aluminum and fused silica windows and air, chopper opening and closing times and phase jitter, measured spectrum and detector efficiencies, sample transmission, multiple scattering and gravity. The results were normalized by the measured flux from the present LANSCE moderator and scaled by the expected performance of a coupled hydrogen moderator at 330 kW proton beam power. Further details of the simulations are given in reference [25].

As much as possible, the same code has been used to compute resolution and intensity at D11. One obvious difference is the neutron source function: the velocity selector at D11 is emulated by a triangular probability distribution with a full-width-half-maximum of 10%. There are no choppers and no gravity focuser, and the time-of-flight is not recorded. When comparing optimum configurations, the cone rule for collimator apertures is applied. When comparing the real experiment, the non-optimum practice of ILL is followed, and there is no aperture at the guide exit. Parameters of the D11 collimation and flux are taken from Lindner *et al.* [26].

5.1 Q-domains and Resolution

Figure 5 illustrates the Q-range and precision for the three new instruments and the present LANSCE LQD compared to simulations of D11. The lines for LANSCE LQD and MQD correspond to the Q-precision for intensity maps obtained using the procedures outlined in section 4 for a binning scheme that optimizes the figure of

merit, Z(Q) = I(Q)/V[Q], for each Q-bin. In figure 5 the box labeled "LQD, Biology LQD" corresponds to the range of rms resolution in Q obtainable using different wavelength bands by changing the phase of the frame-definition chopper. The top of the box corresponds to the earliest phase (smallest λ) and the bottom to the latest phase (largest λ). The four lines for the VLQD in figure 5 represent setting the frame-definition chopper to count in the fifth, fourth, third, or second frames after T_0, while the boxes for D11 correspond to varying the velocity selector between 16 Å (bottom of box) and 4.5 Å (top of box) for different instrument configurations (for the 76-m case, limits are 12 and 6 Å).

[figure 5 here]

The line labeled "LANSCE LQD" in figure 5 shows our computed resolution. The rms Q-resolution at Q = 0.020 $Å^{-1}$ (corresponding to the peak in the measurement of PT5, figure 4) is 0.0023 $Å^{-1}$, while that computed for D11 at 10 m with λ = 10 Å is 0.0020 $Å^{-1}$. We had observed in our previous report [1] that the data from the two instruments were of the same quality, that is that the Q-precision of D11(10m) and the and the LANSCE LQD were the same, which is what we have calculated here. The increase in rms for the LANSCE LQD at higher Q is a consequence of using smaller λ to access these Q-values [7].

The rms Q-resolution of the proposed LQD is comparable to D11 at 21 m total instrument length. However, one should note the large Q-domain, which extends out to 0.4 $Å^{-1}$, that is available on the TOF instruments with a single camera setting. It is possible to extend D11 to Q-values around 0.18 $Å^{-1}$ by configuring the instrument at 5 m and using small λ, but the rms Q-resolution in this configuration is about four times greater than LQD.

MQD will have similar Q-precision to D11(11m) over the dynamic range where the two instruments overlap and roughly two to three times the precision of D11(5m) (not shown) over their common domain. MQD, however, continues out to a maximum Q of about 2.0 $Å^{-1}$.

The Q-precision of the VLQD is very similar to that of D11(76m). The Q-domain of the TOF instrument extends outward to about that attainable for D11(11m), but the resolution is essentially constant for VLQD due to the narrow band of incident neutrons; thus the resolution in this region is considerably better than that for D11.

5.2 Intensities

Figure 6 shows the simulated intensities. The neutron flux on sample is weighted by λ^2 to conserve the area under the histogram in the transformation of $dP/d\Omega$ to dP/dQ. The lines marked D11 correspond to the value for D11 at λ = 10 Å, near the maximum of $\lambda^2\phi$. Our present instrument (LANSCE LQD) is a factor of 2 to 10 lower in intensity than that obtained with the corresponding D11 camera setting. This result is consistent with our previous observation that a measurement on D11 at 10 m took a total of 9 min (including changes in instrument configuration and transmitted beam measurement), while that on LQD took 30 min to obtain the same precision in intensity with the same Q-precision at Q = 0.02 $Å^{-1}$. However, the three-fold wider dynamic range available on the LANSCE LQD makes the actual utility of the instruments comparable. The computed count-rate ratio is within 20% of the observed (which must be considered fortuitous) so that we can be reasonably confident in our comparisons.

The expected intensity for a new LQD on a 330 kW source is 25 times better than the present LANSCE LQD, according to the calculations in figure 6. It will equal that of D11(11m), but will have better resolution by a factor of three. Further, it will have the usual feature of a very large dynamic range. MQD is anticipated to have even higher intensity, somewhere between two to three times higher than D11(11m) with similar Q-precision.

[figure 6 here]

The resolution for VLQD frame 4 is identical to D11(76m) for 10 Å neutrons, so it is appropriate to compare their intensities (figure 6). The computed VLQD intensity is a factor of 2.5 lower, but this is partly due to absorption of the long wavelength neutrons in the detector window. With improved detectors, the intensity (for a

330 kW target) would be very comparable to D11(76m). Thus these simulations show that a VLQD is completely feasible on the proposed high-power pulsed sources. The results compare well with the 76-m configuration of the D11 instrument at ILL in both count rate and Q-precision, due in part to the ability to correct for gravitational effects using the time-of-flight of the detected neutrons.

6. CONCLUSIONS

TOF methods for low-Q measurements have been developed to the point where SANS instruments at relatively modest pulsed spallation sources are now roughly comparable to instruments at high flux reactors. TOF methods have the advantage of a large Q-range (0.002 to 0.4 $Å^{-1}$ for the LANSCE LQD) and ability to correct for wavelength-dependent gravitational droop. Further, the large histograms map into Q with large redundancy but with different Q-precision; thus the trade-off between intensity and Q-precision can be made *after* a measurement to suit the needs of the experiment. The performance of a new generation of instruments on an intense pulsed spallation source, 1 to 5 MW total power, will enable considerable improvement in count rates, Q-precision and Q-domain over existing instrumentation. This enhancement will open new experimental areas in small-angle neutron scattering, extend the range of length scales probed to longer and shorter length scales and enable the design of hybrid instruments able to measure scattering over an even larger domain of length scales from atomic dimensions to hundreds of ångstroms simultaneously.

Acknowledgments

This work was carried out at the Manuel Lujan Jr. Neutron Scattering Center (LANSCE), a national user facility operated by the US Department of Energy under contract W-7405-ENG-36 with the University of California.

REFERENCES

[1] P.A. Seeger and R.P. Hjelm, *J. Appl. Cryst.* **24** (1991), 467–478.

[2] R.P. Hjelm, P.A.Seeger and P. Thiyagarajan, *Proceedings of the 11th Meeting of the International Collaboration on Advanced Neutron Sources*, October 22–26, 1990, Tskuba, Japan. KEK Report 90-25, 673–676.

[3] C.S. Borso, J.M. Carpenter, F.S. Williamson, G.L. Holmblad, H. Mueller, J.J. Faber, J.E. Epperson and S.S. Danyluk, *J. Appl. Cryst.* **15** (1982), 443–448.

[4] Y. Ishikawa, M. Furusaka, N. Nimura, M. Arai and K. Haegawa, *J. Appl.Cryst.* **19** (1986), 229–242.

[5] P.A. Seeger and R. Pynn *Nucl. Instrum. Methods* **A245** (1986), 115–124.

[6] R.P. Hjelm, *J. Appl. Cryst.* **20** (1987), 273–279.

[7] R.P. Hjelm, *J. Appl. Cryst.* **21** (1988), 618–628.

[8] K.K. Crawford and J.W. Carpenter, *J. Appl. Cryst.* **21** (1988), 589–601.

[9] P.A. Seeger, R.P. Hjelm and M. Nutter, *Molecular Crystals Liquid Crystals* **180A** (1990), 101–117.

[10] R.P. Hjelm and P.A. Seeger, *International Seminar on Structural Investigations at Pulsed Neutron Sources*, Joint Institute for Nuclear Physics, Dubna, Russia, (in press) (1993).

[11] G.J. Russell *Proceedings of the 11th Meeting of the International Collaboration on Advanced Neutron Sources*, October 22–26, 1990, Tskuba, Japan. KEK Report 90–25, 335–339.

[12] N. Watanabe, *Conferences in Physics* **97** (1989), 763–769.

[13] N. Watanabe, Y. Kiyanagi, K. Inoue, M. Furusaka, S. Ikeda, M. Arai, H. Iwasa, H., *Conferences in Physics* **97** (1989), 787–797.

[14] Y. Kiyanagi and N. Wanatabe, *Proceedings of the 11th Meeting of the International Collaboration on Advanced Neutron Sources*, October 22–26, 1990, Tskuba, Japan. KEK Report 90–25, 408–414.

[15] M. Furusaka, K.Suzuya, N. Watanabe, M. Osawa, I. Fujikawa and S. Satoh, *International Collaboration on Advanced Neutron Sources XII*, Abingdon, U.K., 24–28 May, 1993.

[16] W. Schmatz, T. Springer, J. Schelten and K. Ibel, *J. Appl. Cryst.* **7** (1974), 96–116.

[17] P.A. Seeger, *Nucl. Instrum. Methods*, **178** (1980), 157–161.

[18] D.F.R. Mildner and J.M. Carpenter, *J. Appl. Cryst.* **17** (1984), 249–256.

[19] A.T. Boothroyd, *J. Appl. Cryst.* **22** (1989) 252–255.

[20] B. Jacrot and G. Zaccai, *Biopolymers* **20** (1981), 2413–2426.

[21] G.D. Wignal and F.S. Bates, *J. Appl. Cryst.* **20** (1987), 28–40.

[22] R.E. Ghosh and A.R. Rennie, *Conferences in Physics* **107** (1990), 233–244.

[23] A.R. Rennie and R.K. Heenan, *International Seminar on Structural Investigations at Pulsed Neutron Sources*, Joint Institute for Nuclear Physics, Dubna, Russia, (in press) (1993).

[24] J.R.D. Copley, *J. Appl. Cryst.* **21** (1988), 639–644.

[25] P.A. Seeger and R.P. Hjelm, *International Collaboration on Advanced Neutron Sources XII*, Abingdon, U.K., 24–28 May, 1993.

[26] P. Lindner, R.P. May and P.A. Timmins, *Physica* **B 180&181** (1992), 967–972

Figure Legends:

Figure 1. Generalized diagram of a low-Q diffraction instrument for a pulsed spallation neutron source. The nomenclature is discussed in the text. This geometry has been used in the design of a family of diffractometers for a new high-power source.

Figure 2. A map of raw data from the vycor glass sample, PT5, as a function of time-of-flight and detector radius. The counts are displayed on a logarithmic scale in positive contrast (highest counts brightest). For a color rendition as presented to the user see reference [1].

Figure 3. Absolute differential scattering probability, $dP/d\Omega$, mapped on Q and λ for a vycor glass sample. The data shown in figure 2 are normalized and mapped into Q–λ space. The data below the white line are excluded because the Q-precision is poor.

Figure 4. Radially averaged Q-Map of the vycor glass sample PT5 The data have been averaged over λ. Note that statistical errors in both Q and $dP/d\Omega$ are propagated for all points.

Figure 5 Computed statistical resolution in Q as a function of Q for a number of SANS instruments. The various D11 configurations and the LQD/biology LQD are shown as boxes representing continuous choices of wavelength. The present LQD and the proposed MQD record all wavelengths at a single setting, and the VLQD is expected to be operated at a few selected wavelengths.

Figure 6. Intensity of SANS instruments weighted by λ^2. Only instruments with the same resolution on figure 5 should be compared; *e.g.*, MQD and D11(11 m), Biology LQD and D11(21 m), or VLQD frame 4 and D11(76 m).

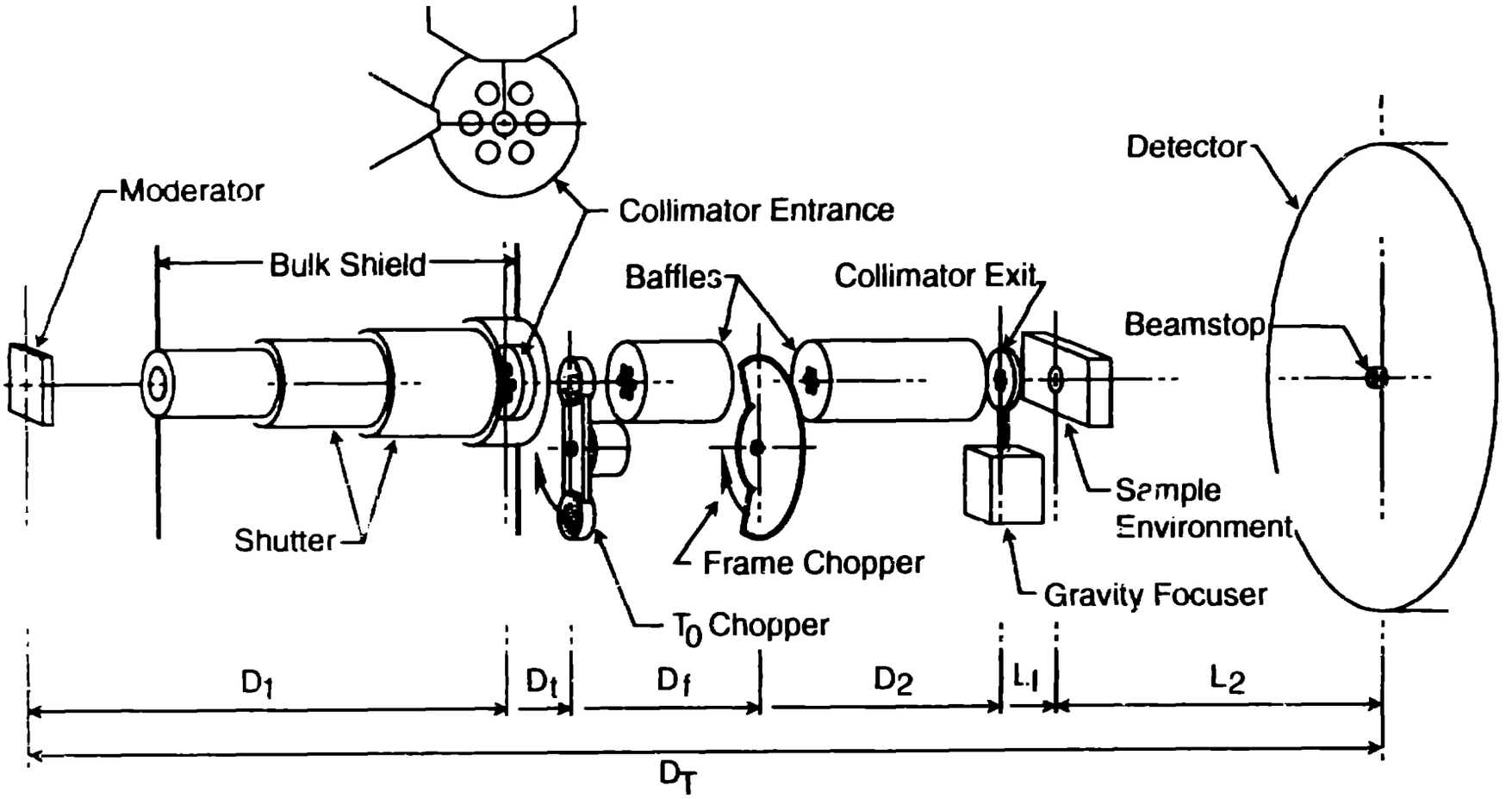
Moderator
Bulk Shield
Collimator Entrance
Baffles
Collimator Exit
Detector
Beamstop
Shutter
Frame Chopper
Sample Environment
Gravity Focuser
T_0 Chopper
D_1
D_t
D_f
D_2
L_1
L_2
D_T

Fig. 1

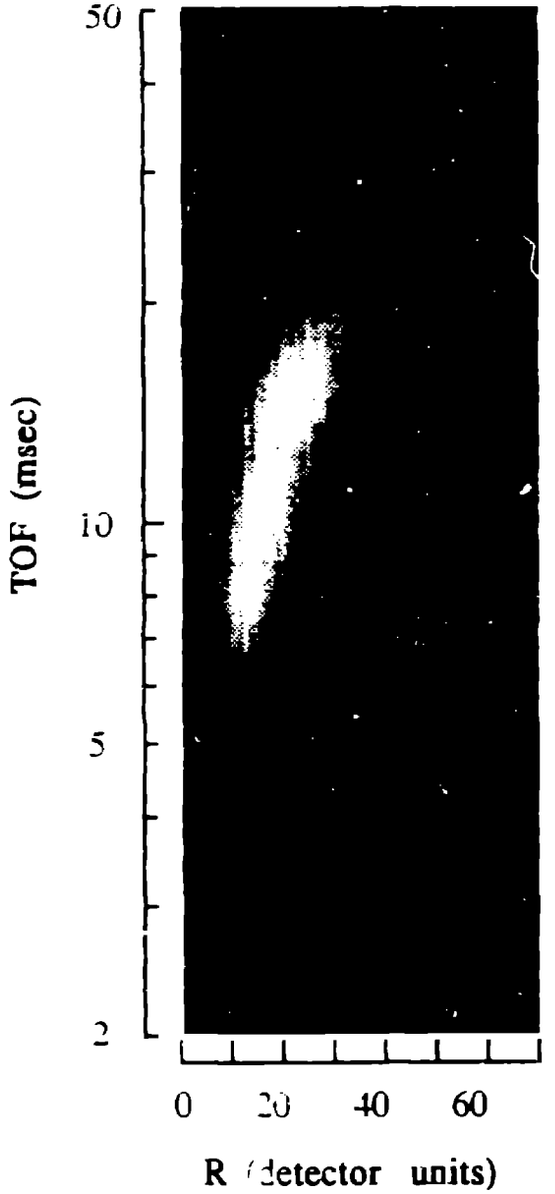
50
10
5
2
TOF (msec)
0
20
40
60
R (detector units)

Fig. 2

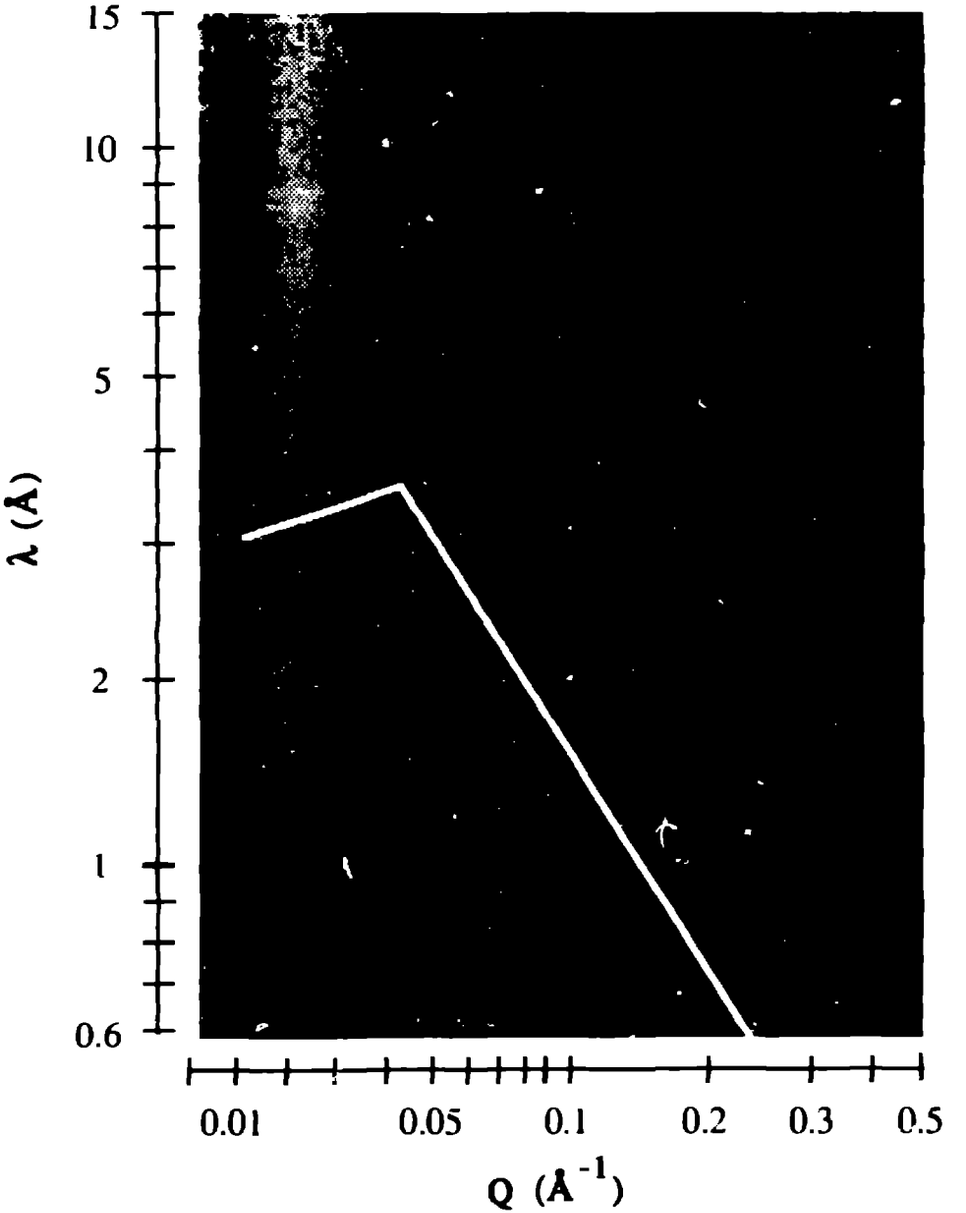
15
10
5
2
1
0.6
λ (Å)
0.01
0.05
0.1
0.2
0.3
0.5
Q (Å^{-1})

Fig. 3

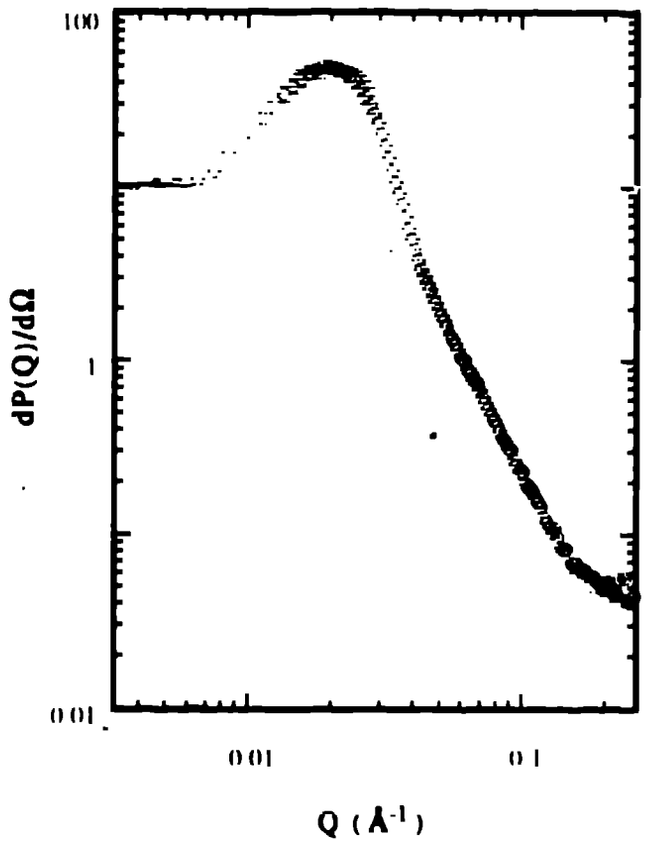

Fig. 4

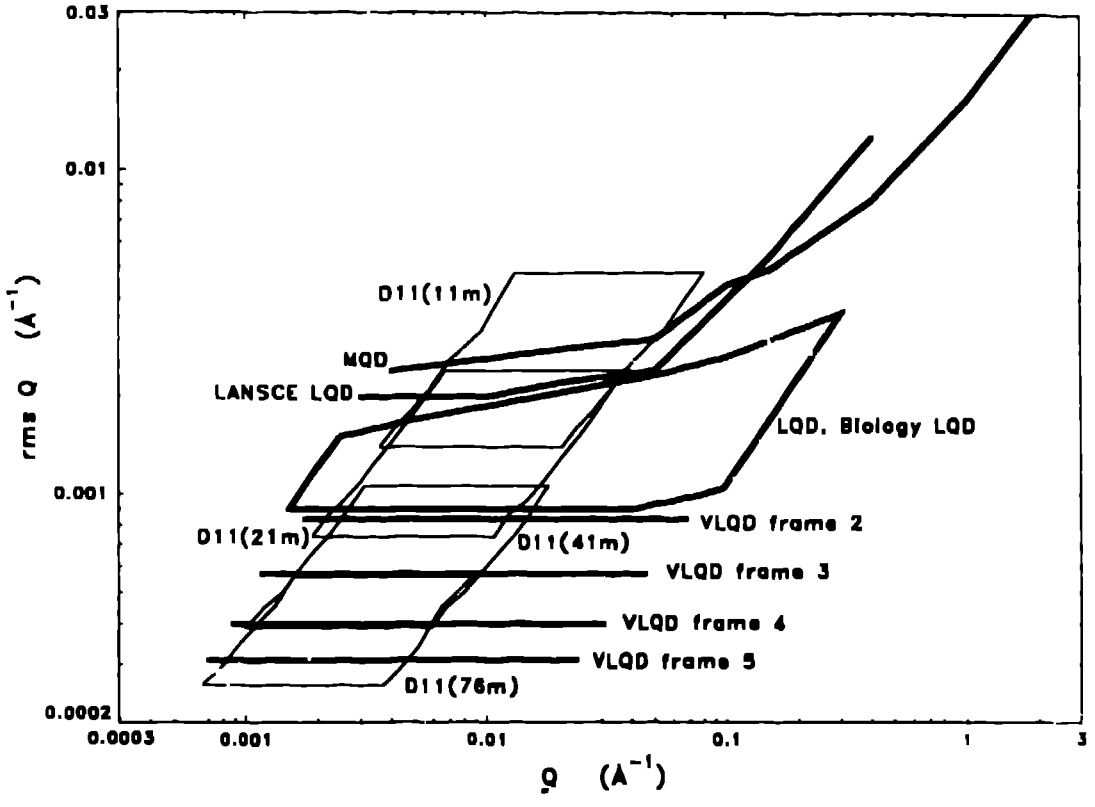
0.03
0.01
0.001
0.0002
rms Q (Å⁻¹)
0.0003
0.001
0.01
0.1
1
3
Q (Å⁻¹)
D11(11m)
MQD
LANSCE LQD
LQD, Biology LQD
VLQD frame 2
D11(21m)
D11(41m)
VLQD frame 3
VLQD frame 4
VLQD frame 5
D11(76m)

Fig. 5

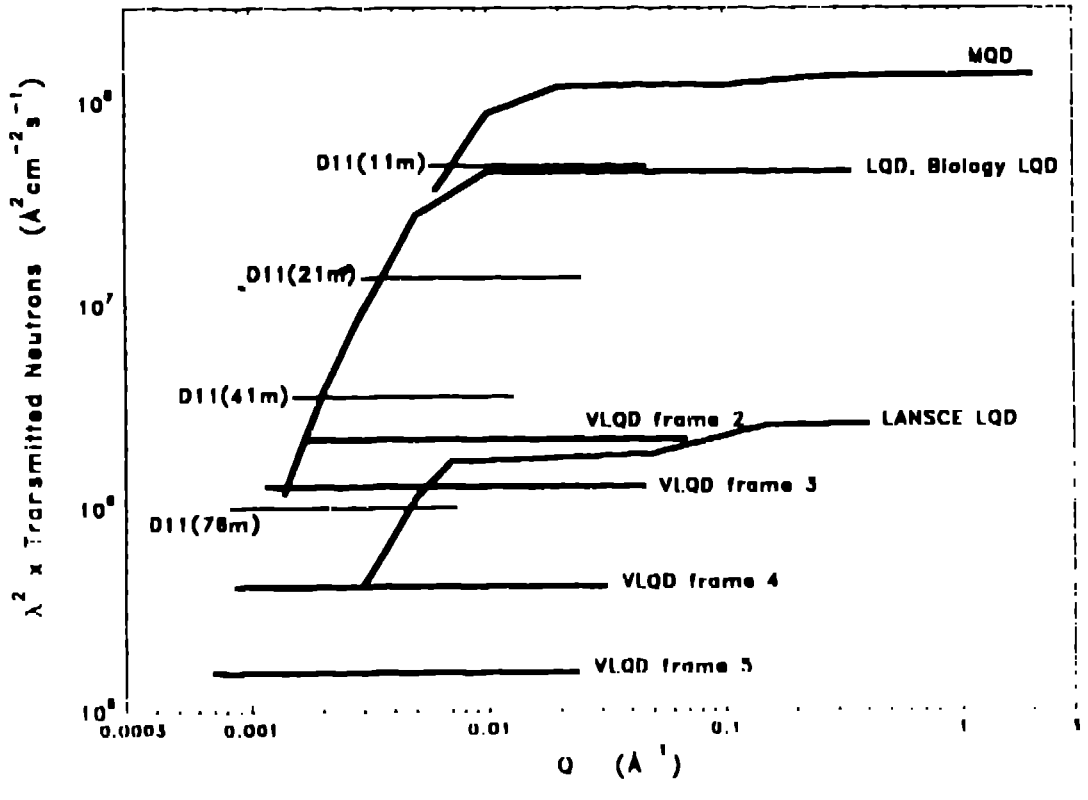
λ² x Transmitted Neutrons (Å²cm⁻²s⁻¹)
10⁸
10⁷
10⁶
10⁵
0.0003
0.001
0.01
0.1
1
Q (Å⁻¹)
MQD
D11(11m)
LQD, Biology LQD
D11(21m)
D11(41m)
VLQD frame 2
LANSCE LQD
VLQD frame 3
D11(76m)
VLQD frame 4
VLQD frame 5

Fig. 6